Journal of the Korean Magnetic Resonance Society **2022**, *26*, 46-50
DOI 10.6564/JKMRS.2022.26.4.046

Backbone hydrogen bonding interaction of the inactive isoform of type III antifreeze proteins studied by $^{1}H/^{15}N$-HSQC spectra

Seo-Ree Choi, Sung Kuk Kim, Jaewon Choi, and Joon-Hwa Lee*

Department of Chemistry and RINS, Gyeongsang National University, Jinju 52828, Republic of Korea

Received Nov 30, 2022; Revised Dec 13, 2022; Accepted Dec 13, 2022

Abstract Antifreeze proteins (AFPs) bind to the ice crystals and then are able to inhibit the freezing of body fluid at subzero temperatures. Type III AFPs are categorized into three subgroups, QAE1, QAE2, and SP isoforms, based on differences in their isoelectric points. We prepared the QAE2 (AFP11) and SP (AFP6) isoforms of the notched-fin eelpout AFP and their mutant constructs and determined their temperature gradients of amide proton chemical shifts ($\Delta\delta/\Delta T$) using NMR. The nfeAFP11 (QAE2) has the distinct $\Delta\delta/\Delta T$ pattern of the first 3_{10} helix compared to the QAE1 isoforms. The nfeAFP6 (SP) has the deviated $\Delta\delta/\Delta T$ values of many residues, indicating its backbone conformational distortion. The study suggests the distortion in the H-bonding interactions and backbone conformation that is important for TH activities.

Keywords NMR, thermostability, backbone stability, antifreeze protein, ice-binding protein

Introduction

Antifreeze proteins (AFPs) are capable of depressing the freezing point (T_f) of body fluid below the melting point (T_m) to promote the survival of living organisms at subzero temperatures.[1-4] The type III AFPs have been categorized into two sub-groups, quaternary-amino-ethyl (QAE) and sulfopropyl (SP) Sephadex-binding isoforms, based on differences in their isoelectric points, and the QAE proteins can be further divided into QAE1 and QAE2 subgroups.[5] The Japanese notched-fin eelpout (*Zoarces elongates Kner*) produces 13 different isoforms of type III AFP (denoted nfeAFP1 – nfeAFP13), which have been divided into six SP (nfeAFP1 – nfeAFP6), four QAE1 (nfeAFP7 – nfeAFP10), and three QAE2 (nfeAFP11– nfeAFP13) isoforms. The QAE1 isoforms exhibit full thermal hysteresis (TH) activity and can completely arrest ice crystal growth at temperatures below the T_f of a solution. In contrast, the SP and QAE2 isoforms are incapable of preventing the growth of ice crystals and thus have extremely low or no TH activity. The ice-binding surface (IBS) of a type III AFP is composed of solvent-exposed residues from two parts of the amino acid sequence (residues 9–21 and 41–44; Fig. 1A). The IBS consists of two adjacent surfaces, which bind to the pyramidal and primary prism planes of the ice crystal, respectively.[6] And the relative hydrophobicity and flatness of the IBS are thought to be important for antifreeze activity. The SP isoform (nfeAPF6) and QAE2 isoform (nfeAFP11) from Japanese notched-fin eelpout could be converted into active mutants (nfeAPF6_tri and nfeAFP11_tri) obtained by changing the IBS with the corresponding residues of QAE1, which exhibits TH effects similar to those of its paralogue QAE1.[7-9] The nfeAFP6_tri (P19L/A20V/G42S) and nfeAFP11_tri

* Address correspondence to: **Joon-Hwa Lee,** Department of Chemistry and RINS, Gyeongsang National University, Jinju 52828, Republic of Korea, Tel: 82-55-772-1490; Fax: 82-55-772-1489; E-mail: joonhwa@gnu.ac.kr

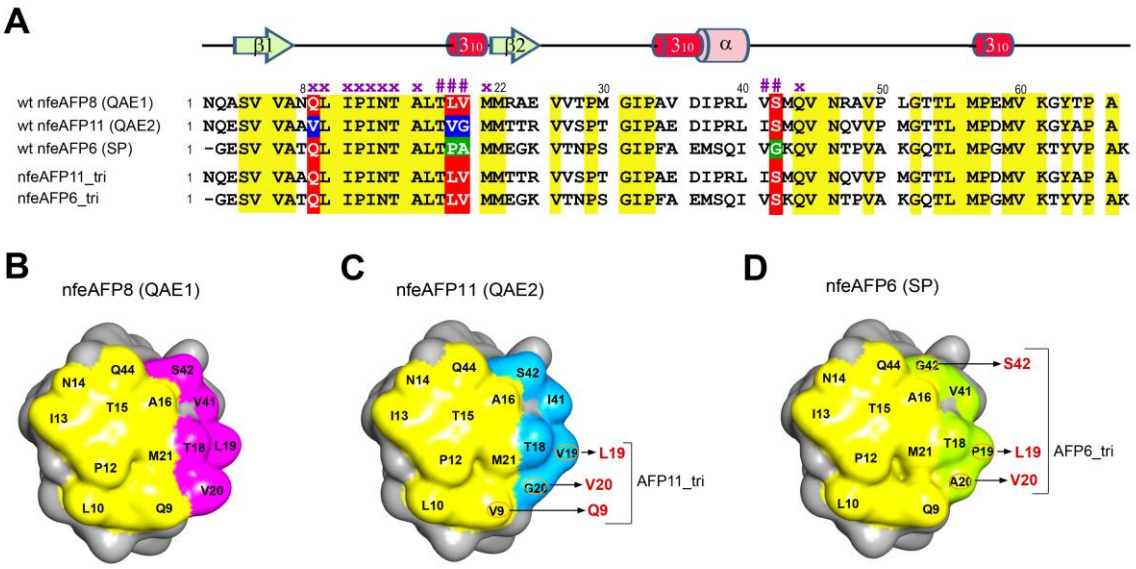

Figure 1. (A) Multiple sequence alignment of the type III AFPs. nfeAFP6, nfeAFP8, and nfeAFP11 are the isoforms 6, 8, and 11 of the notched-fin eelpout type III AFP, respectively. Yellow bars indicate invariant or nearly invariant residues in the type III AFP family. Red, blue, and green bars indicate variant residues in the IBS of type III AFPs. The x and # symbols represent residues composing the pyramidal and primary prism plane-binding surfaces, respectively. IBS of (B) the QAE1 isoform, (C) QAE2 isoform, and (D) SP isoform of type III AFPs. The surfaces binding to the pyramidal plane of ice are colored yellow and the surfaces binding to the primary prism plane of ice are colored magenta, cyan, or green.

(V9Q/V19L/G20V) mutants were structurally compared with QAE1 (Fig. 1B). To understand the antifreeze activity of nfeAFP isoforms, we performed NMR experiments on wild-type (wt) nfeAFP6, nfeAFP11, and two mutants.[10] We characterized the structural properties of the IBS of the wt and mutant by analyzing the temperature gradient of the amide proton chemical shift and its correlation with the chemical shift deviation (CSD) from random coil. Structural changes were observed in the active QAE1-like mutants compared to the fully active wt QAE1 isoform. Our structural studies provide valuable insights into the molecular mechanism of the antifreeze activity of type III AFPs.

Experimental Methods

Sample preparation- The DNA coding sequences for the wt nfeAFP11 and wt nfeAFP6 and their mutants, nfeAFP11_tri and nfeAFP6_tri, were purchased from BIONEER Inc. (Daejeon, Korea) and cloned into *E. coli* expression vector pET28a, which has an N-terminal His-tag. To produce uniformly ^{15}N-labeled wt and mutant nfeAFPs, BL21(DE3) cells were grown in an M9 minimal medium that contained 1 g/L $^{15}NH_4Cl$ as the sole nitrogen source. The ^{15}N-labeled proteins were purified by a Ni-NTA affinity column and a Sephacryl S-100 gel filtration column on a GE AKTA FPLC (GE Healthcare, Chicago, IL, USA). The protein samples were dissolved in a 90% H_2O/10% D_2O buffer containing 10 mM sodium phosphate (pH 6.0) and 100 mM NaCl. The concentrations of protein samples were determined using a Pierce BCA Protein Assay Kit (Thermo Fisher, Scientific, Waltham, MA, USA).

NMR experiments- All of the ^{1}H and ^{15}N NMR experiments were performed on an Agilent DD2 700-MHz NMR spectrometer (GNU, Jinju, Korea)

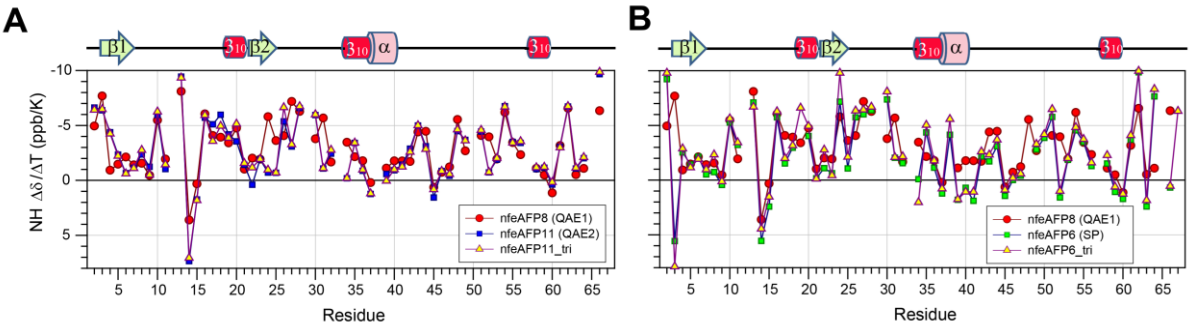

Figure 2 Temperature gradients of amide proton chemical shifts (Δδ/Δ*T*) of (A) wt nfeAFP11 and nfeAFP11_tri and (B) wt nfeAFP6 and nfeAFP6_tri as a function of residue number.

equipped with a triple-resonance probe. All two-dimensional (2D) $^{1}H/^{15}N$-HSQC experiments were carried out with samples of 1 mM ^{15}N-labeled wt and mutant nfeAFPs at 5 °C ~ 25 °C. 2D data were processed with the program NMRPIPE[11] and analyzed with the program NMRFAM-Sparky.[12] The Δδ/Δ*T* values of the amide protons were determined from linear variation of the NH chemical shifts with temperature. The amide proton CSDs ($\delta_{obs} - \delta_{rc}$) at 25 °C were calculated from the observed chemical shifts (δ_{obs}) and the corresponding random coil (δ_{rc}) values taken from the literature.[13]

Results and Discussion

Temperature gradients - The amide chemical shifts of proteins are sensitive to the environment of the observed nuclei and provide information about temperature-related structural or dynamic changes.[14,15] Fig. 2A shows the temperature gradients of amide proton chemical shifts (Δδ/Δ*T*) in the wt nfeAFP11 (QAE2) and nfeAFP11_tri which were compared with those of wt nfeAFP8 (QAE1). As temperature decreases, the water signal is downfield shifted and the Δδ/Δ*T* value of water is –4.6 ppb·K^{-1}. Many residues have Δδ/Δ*T* values > –4.6 ppb·K^{-1}, indicating that these amides are H-bonded.[16,17] Conversely, the Δδ/Δ*T* values < –4.6 ppb·K^{-1} indicate that the amide protons of these residues were not protected from the exchange by H-bonding. In all of the proteins, residues N14, T15, I37, V45, and V60 have Δδ/Δ*T* values > 0 ppb·K^{-1}, similar to the QAE1 isoform AFP HPLC12 from the ocean pout (*Macrozoarces americanus*).[18] In T18, V20, and M22 clear differences are observed and nfeAFP11_tri shows a similar pattern to nfeAFP8. In other residues, there are no clear differences nfeAFPs.

Fig. 2B shows the Δδ/Δ*T* in the wt nfeAFP6 (SP) and nfeAFP6_tri compared with wt nfeAFP8 (QAE1). The overall pattern of the Δδ/Δ*T* values in nfeAFP6 and nfeAFP6_tri was similar to each other. In both of nfeAFP6 and nfeAFP6_tri, residues E3, F34, I40, V41, G52, M59, Y63 and A66 have Δδ/Δ*T* values > 0 ppb·K^{-1}. However, it was a little different from nfeAFP8, probably the difference in isoelectric points. Nevertheless, in A7, T8, V20, M22, and Q44 some differences are observed and nfeAFP6_tri shows a similar pattern to nfeAFP8. The overall patterns of the Δδ/Δ*T* values in all proteins were very similar to each other, although each mutation slightly affected the residues in the first 3_{10} helices (T18–M22).

Chemical shift deviation – Previous statistical studies reported that the Δδ/Δ*T* values exhibited a linear correlation with their CSD values.[17] To characterize in detail the structural and dynamic properties of the wt and mutant nfeAFPs, a combined analysis of Δδ/Δ*T* values with CSD was performed, and correlation plots are shown in Fig. 3. In all proteins, residues I11, N14, T15, and S42/G42 of the IBS have Δδ/Δ*T* values significantly lower than the statistical correlation line between Δδ/Δ*T* and CSD (Δδ/Δ*T* =

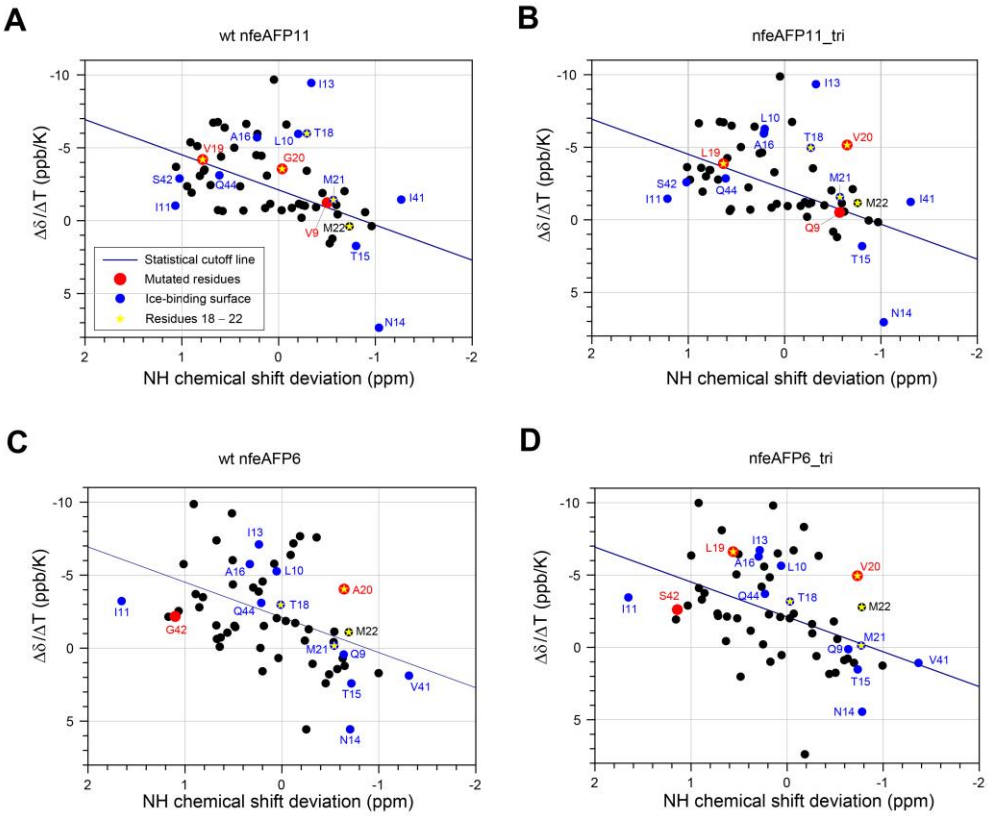

Figure 3. The amide proton $\Delta\delta/\Delta T$ – CSD correlation plots of (A) wt nfeAFP11, (B) nfeAFP11_tri, (C) wt nfeAFP6, and (D) nfeAFP6_tri. Solid lines indicate the statistical cutoff, $\Delta\delta/\Delta T = -2.41 \times \text{CSD} - 2.11$. The residues composing the ice-binding surface are shown in blue. The residues at mutation sites are highlighted in red.

–2.41 × CSD – 2.11) (Fig. 3). These results indicate that these residues contributed to stabilizing the IBS via strong H-bonding interactions and slowly exchanged with solvent water. In contrast, their neighboring residues, L10, I13, and A16 were above the statistical cutoff line, suggesting that these residues are not H-bonded and rapidly exchanged with solvent water.

In wt nfeAFP11, the residues in the first 3_{10} helix (T18–M22) show a unique pattern of $\Delta\delta/\Delta T$ (Fig. 3A). Residue T18 has significantly larger $\Delta\delta/\Delta T$ values than the statistical cutoff line, while residues L19 and M21 are located near the cutoff line (Fig. 3A). The CSD value of G20 in nfeAFP11 is ~ 0 and then G20 is close to the statistical cutoff line (Fig. 3A). However, in nfeAFP11_tri, the CSD of the corresponding V20 of is less than -0.6 ppm (Fig. 3B). As a result, residue V20 is more deviated from the cutoff line compared to G20 of nfeAFP11 (Fig. 3). The similar results were observed for nfeAFP8 and its triple mutant, nfeAFP8_tri.[9] These data indicated that the replacement of G20 in nfeAFP11 with valine recovers the H-bonding interactions within the first 3_{10} helix like those of the QAE1 isoform, nfeAFP8.

In wt nfeAFP6 and nfeAFP_tri, the residues in the first 3_{10} helices (T18-M22) show a similar pattern of $\Delta\delta/\Delta T$ to nfeAFP11_tri (Fig. 3C, D). However, unlike nfeAFP11 (Fig. 3A, B) and nfeAFP8,[9] many residues of nfeAFP6 are located at different positions from those of nfeAFP6_tri (Fig. 3C, D). These data indicated that nfeAFP6_tri exhibit a distinct backbone conformation compared to wt nfeAFP6,

even though these two proteins have similar H-bonding interaction patterns to each other.

In summary, we determined the $\Delta\delta/\Delta T$ values of the wild-type notched-fin eelpout AFP and their mutant AFP using NMR spectroscopy. The $\Delta\delta/\Delta T$ pattern of the first 3_{10} helix in nfeAFP11 (QAE2 isoform) is quite different (especially, G20) from those of nfeAFP8 (QAE1 isoform) and nfeAFP11_tri (QAE1-like), indicating the disruption of H-bonding interaction in the first 3_{10} helix of QAE2 isoforms. In the SP isoform, nfeAFP6, the $\Delta\delta/\Delta T$ values of the first 3_{10} helix showed a similar pattern to the QAE1 isoform. Instead, the distinct CSD values of many residues in wt nfeAFP6 indicated the structural distortion of its backbone conformation. This study suggests the distortion in the H-bonding interactions and backbone conformation that is important for TH activities.

Acknowledgments

This work was supported by grants from the National Research Foundation of Korea (2020R1A2C1006909 and 2022R1A4A1021817) and the Samsung Science and Technology Foundation (SSTF-BA1701-10).

References

1. Y. Yeh and R. E. Feeney, *Chem. Rev.* **96**, 601 (1996)
2. K.V. Ewart, Q. Lin, and C. L. Hew, *Cell. Mol. Life Sci.* **55**, 271 (1999)
3. G. L. Fletcher, C. L. Hew, and P. L. Davies, *Annu. Rev. Physiol.* **63**, 359 (2001)
4. Z. Jia and P. L. Davies, *Trends Biochem. Sci.* **27**, 101 (2002)
5. Y. Nishimiya, R. Sato, M. Takamichi, A. Miura, and S. Tsuda, *FEBS J.* **272**, 482 (2005)
6. C. P. Garnham, Y. Nishimiya, S. Tsuda, and P. L. Davies, *FEBS Lett.* **586**, 3876 (2012)
7. C. P. Garnham, R. L. Campbell, and P. L. Davies, *Proc. Natl. Acad. Sci. USA* **108**, 7363 (2011)
8. S. Mahatabuddin, D. Fukami, T. Arai, Y. Nishimiya, R. Shimizu, C. Shibazaki, H. Kondo, M. Adachi, and S. Tsuda, *Proc. Natl. Acad. Sci. USA* **115**, 5456 (2018)
9. S.-R. Choi, Y.-J. Seo, M. Kim, Y. Eo, H.-C. Ahn, A.-R. Lee, C.-J. Park, K.-S. Ryu, H.-K. Cheong, S. S. Lee, E.S. Jin, and J.-H. Lee, *FEBS Lett.* **590**, 4202 (2016)
10. S.-R. Choi, J. Lee, Y.-J. Seo, H. S. Kong, M. Kim, E.S. Jin, J. R. Lee, and J.-H. Lee, *Comput. Struct. Biotechnol. J.* **19**, 897 (2021)
11. F. Delaglio, S. Grzesiek, G. W. Vuister, G. Zhu , J. Pfeifer, and A. Bax, *J. Biomol. NMR* **6**, 277 (1995)
12. W. Lee, M. Tonelli, and J. L. Markley. *Bioinformatics* **31**, 1325 (2015)
13. N. H. Andersen, J. W. Neidigh, S. M. Harris, G. M. Lee, Z. Liu, and H. Tong, *J. Am. Chem. Soc.* **119**, 8547 (1997)
14. M. Ohnishi and D. W. Urry, *Biochem. Biophys. Res. Commun.* **36**, 194 (1969)
15. J. Hong, Y. Hu, C. Li, Z. Jia, B. Xia, and C. Jin, *PLoS One* **5**, e15682 (2010)
16. T. Cierpicki and J. Otlewski, *J. Biomol. NMR* **21**, 249 (2001)
17. T. Cierpicki, I. Zhukov, R. A. Byrd, and J. Otlewski, *J. Magn. Reson.* **157**, 178 (2002)
18. Y.-G. Choi, C.-J. Park, H.-E. Kim, Y.-J. Seo, A.-R. Lee, S.-R. Choi, S. S. Lee, and J.-H. Lee, *J. Biomol. NMR* **61**, 137 (2015)